

## Supplemental Information

### Understanding the Activity of Glucose Oxidase after Exposure to Organic

### Solvents

*Vygailė Dudkaitė<sup>a</sup>, Visvaldas Kairys<sup>b</sup>, Gintautas Bagdžiūnas<sup>a</sup>*

<sup>a</sup> Group of Supramolecular Analysis, Institute of Biochemistry, Life Sciences Centre, Vilnius University, Saulėtekio av. 7, LT-10257, Vilnius, Lithuania

<sup>b</sup> Department of Bioinformatics, Institute of Biotechnology, Life Sciences Centre, Vilnius University, Saulėtekio av. 7, LT-10257, Vilnius, Lithuania

\*Correspondence: [gintautas.bagdziunas@gmc.vu.lt](mailto:gintautas.bagdziunas@gmc.vu.lt) (ORCID ID: 0000-0002-9924-6902)

#### Table of Contents

Materials.....	S2
Instrumentation.....	S2
Sample preparation.....	S3
Enzyme assay.....	S3
Correlation between the solvent properties and the GOx catalytic efficiencies.....	S4
Computational Details.....	S7
References.....	S11



**Materials.** The organic solvents were purchased from Eurochemicals and distilled prior the experiments. The used lyophilized powder enzymes of type VII glucose oxidase (GOx) from *Aspergillus niger* of  $\geq 100$  U mg<sup>-1</sup> (without added oxygen) and type I peroxidase from horseradish (HRP) of approximately 150 U mg<sup>-1</sup> were purchased from Sigma Aldrich. All inorganic salts for the buffer solutions were purchased from Carl Roth GmbH + Co. KG.

**Instrumentation.** Ultraviolet–visible (UV-Vis) spectra were measured to evaluate the kinetic constants using an Evolution 300 Security UV-Vis Spectrophotometer (Thermo Fisher Scientific). During the measurements, the samples were thermostated at 25 °C using an integrated thermostat. A JASCO J-815 Circular Dichroism spectrometer (Tokyo, Japan) was used to measure the circular dichroism (CD) spectra of GOx prior and after exposure to organic solvents. These CD spectra were carried out under a stream of Ar gas (5 L min<sup>-1</sup>) and in a wavelength range of 190-500 nm with a scan rate of 50 nm min<sup>-1</sup>, the concentration of GOx solutions were 1.0 mg mL<sup>-1</sup>. The CD spectra were recorded two times and the results were averaged and the baseline was subtracted. The path length of cell was 0.10 cm.

Hydrodynamic diameter of nanoparticles was measured using Zetasizer  $\mu$ V (Malvern) and its compatible software. DMF, DMSO, THF, AN, CHF and buffer solutions of GOx (concentration of 1 mg mL<sup>-1</sup>) were observed. Prior to the experiment, the solutions were filtered using membrane syringes (CA 0.45  $\mu$ m) to get reliable particle size data and remove large dust particles. Because GOx nanoparticles were measured in pure DMF and DMSO, the solvent parameters in the software were changed from water to DMF and DMSO, respectively. This required to define the solvents by their temperature, viscosity and refractive index. The measurements were performed 3 times and averaged by the program.

**Sample preparation.** The native GOx enzyme was dissolved in potassium phosphate buffer (NaH<sub>2</sub>PO<sub>4</sub> - Na<sub>2</sub>HPO<sub>4</sub>) of pH 7.0 (50 mM) and used as a standard of activity comparison. The samples of GOx in organic solvents of 1.0 mg mL<sup>-1</sup> were dissolved using a Professional Grade Ultrasonic Cleaner P4820-WPT (iSonic) bath. Before the experiments, the samples in organic solvents were kept for 24 h in the refrigerator at 4 °C. The solvents, which can be evaporated without the enzyme denaturation, i.e., in temperature lower than 40 °C, were removed using a vacuum rotary evaporator and dissolved in the buffer to the concentration of 1.0 mg mL<sup>-1</sup>. To check that these solvents have no effect to these experiments, samples of 10 µL of the solutions of GOx in *N,N*-dimethylformamide (DMF) and dimethyl sulfoxide (DMSO) were used in the experiments.

**Enzyme assay.** GOx activity was measured with the aid of a coupled *o*-dianisidine-peroxidase reaction using the UV-Vis spectroscopy.<sup>1</sup> Prior to these experiments, the 1.0 M glucose solution in the buffer was allowed to mutarotate overnight. The reaction mixture contained from 2 to 600 µL of 1.0 M *D*-glucose solution, 10 µL of 20 mM solution of *o*-dianisidine in ethanol, 50 µL of 5 mg mL<sup>-1</sup> solution HRP in the buffer, in a cuvette with the 50 mM buffer of pH 7.0. The total volume of the tested solution was 2.1 mL. In the mixture, 10 µL of 1.0 mg mL<sup>-1</sup> test solution of GOx was added and the mixture was stirred for 5 s. The linear rate of glucose consumption was determined from the rate of absorption at 460 nm for 30 s using the UV-Vis spectrophotometer, thermostated at 25°C. The amount of glucose oxidized at each time interval was plotted versus time. The slope of each curve was determined to obtain the initial velocity for each glucose concentration. The initial velocity for each glucose concentration was estimated using this equation (S2):

$$V = \frac{1}{\epsilon \times l} \times \frac{dA}{dt} \times 10^6 \quad (\text{S2})$$

where  $V$  is an initial velocity ( $\mu\text{M s}^{-1}$ );  $\frac{dA}{dt}$  is a mathematical differential of UV-Vis absorption  $A$  versus time or the certain points in time, where both points align on the same trend line;  $\varepsilon$  is the molar extinction coefficient of oxidized *o*-dianisidine at 460 nm ( $11300 \text{ L mol}^{-1} \text{ cm}^{-1}$ );  $l$  equals the path length (1.0 cm). All the experiments were conducted using type II water ( $R > 18 \text{ M}\Omega$ ) purified in a Milli-Q system.

The obtained initial velocity ( $V$ ) versus the glucose concentration curves were used to calculate the Michael – Menten constants ( $K_M$ ), and the catalytic rate constants ( $k_{cat}$ ) by applying the Michaelis–Menten equation (S3):

$$V = \frac{k_{cat}[GOx][Glu]}{K_M + [Glu]} \quad (\text{S3})$$

where  $[GOx]$  is total concentration of the one GOx subunit of  $6.0 \times 10^{-8} \text{ M}$  in the reaction solution, which was measured based on UV-vis spectra of GOx in the pH = 7.0 buffer at 280 nm using a extinction coefficient of  $2.7 \times 10^5 \text{ M}^{-1} \text{ cm}^{-1}$ .<sup>2</sup> These kinetic parameters ( $K_M$  and  $k_{cat}$ ) for the reaction of the *o*-dianisidine oxidation were calculated by employing the Origin software.

**Correlation between the solvent properties and the GOx catalytic efficiencies.** To estimate this correlation between the catalytic efficiencies and the solvents physical properties, the least squares of the experimental and calculated catalytic efficiencies method by Eq. 1 was used. Solver as the Microsoft Excel add-in program was employed.

Table S1. Diameters of the aggregates and the physical properties such as the polarity of the solvent, the energies of intermolecular interaction between the solvent and the peptide residues, the tendency of the organic solvent to adsorb to lipids of the used solvents, and experimental and calculated catalytic efficiencies of GOx.

<i>Entry</i>	<i>Solvent</i>	$\bar{d}$ , nm	<i>P</i>	$-E_i$ , kJ mol <sup>-1</sup>	log $K_{ow}$	<i>Exper.</i> $k_{cat}/K_M$ (mM <sup>-1</sup> s <sup>-1</sup> )	<i>Calc.</i> <sup>a</sup> $k_{cat}/K_M$ (mM <sup>-1</sup> s <sup>-1</sup> ) <sup>a</sup>
1	Buffer	22	10.2	36.4	-	9.6 ± 0.2	10.0 ± 0.3
2	CHF	280	4.1	6.84	1.97	6.4 ± 0.2	5.6 ± 0.3
3	DCM	180	3.1	7.87	1.25	3.8 ± 0.3	3.0 ± 0.3
4	DCE	230	3.7	7.86	1.48	3.5 ± 0.2	3.9 ± 0.3
5	THF	460	4.2	25.5	0.46	5.4 ± 0.2	5.4 ± 0.3
6	DME	380	3.5	23.8	-0.21	2.3 ± 0.1	2.9 ± 0.3
7	PhMe	200	2.4	8.20	2.73	2.7 ± 0.1	2.9 ± 0.3
8	AN	300	5.8	21.3	-0.34	3.9 ± 0.2	3.8 ± 0.3
9	EA	290	4.3	25.9	0.73	4.7 ± 0.1	3.4 ± 0.3
10	EtOH	190	5.2	23.5	-0.24	2.3 ± 0.1	2.6 ± 0.3
11	DMSO	280	7.2	31.6	-1.35	-	3.1 ± 0.3
12	DMF	460	6.4	27.0	-1.01	-	5.8 ± 0.3
13	Et <sub>2</sub> O	~200	2.8	26.5	0.89	2.2 ± 0.1	1.9 ± 0.3

<sup>a</sup> – a confidence interval for all results is calculated using confidence of 0.95 and n = 10.

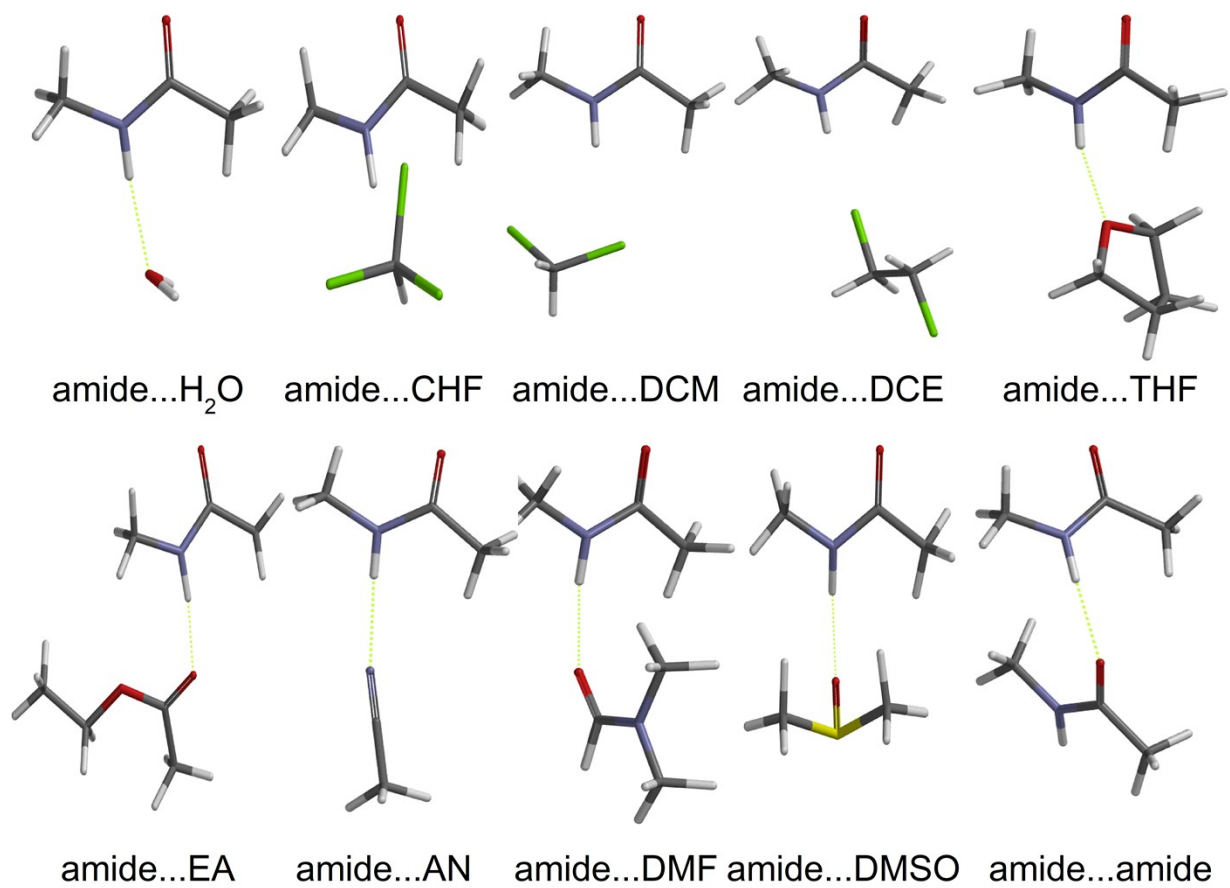


Figure S1. Optimized geometries with intermolecular H-bonds between the solvents and the amide bond.

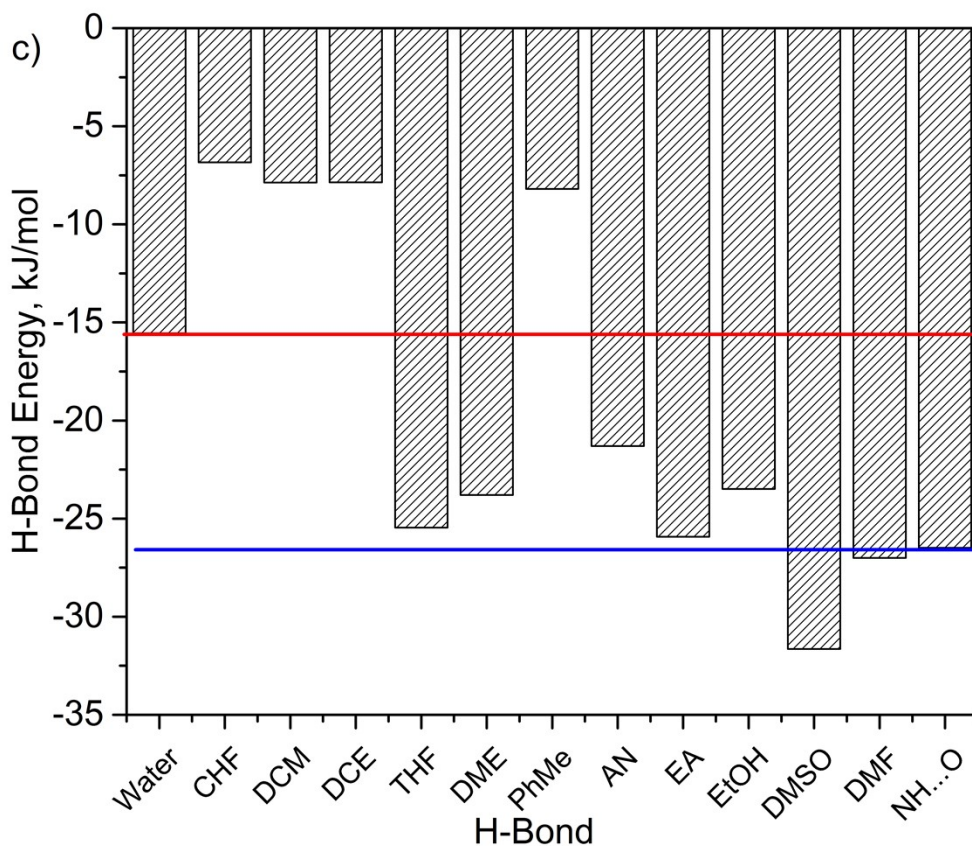


Fig. S2. The computed interaction energies between amide and various solvents or species (including NH...O as the amide-amide interaction).

**Computational Details.** The molecular dynamics (MD) simulations of the protein in various solvents were performed using a GROMACS (v. 2020.4) program.<sup>3</sup> A CHARMM36 force field (February 2021 version) with a CHARMM36m parameter set for proteins was used for the simulations.<sup>4</sup> The parameters for the missing solvent species were generated using a CGenFF (v. 4.4) server.<sup>5</sup> Some solvents were left out of the simulations because of the lack of suitable parameters, or severe equilibration problems. The CHARMM-compatible parameters by Aleksandrov were used for FAD.<sup>6</sup>

Before placing a protein into the organic solvents, MD equilibration of the pure solvent box were performed. A 100×100×100 Å cubic box was filled with a number of solvent molecules



corresponding to the experimental density at 293 K. The system was first subjected to a steepest descents minimization until the maximum force on any of the atoms decreased to less than 1000  $\text{kJ}\cdot\text{mol}^{-1}\text{ nm}^{-1}$ . Afterwards, the pure solvent box was subjected to a 100 ps *NVT* equilibration (i.e., in this canonical ensemble, amount of substance (N), volume (V) and temperature (T) are conserved) using 2 fs time steps at 293 K temperature. Finally, 20 ns *NPT* equilibration (i.e., in this isothermal–isobaric ensemble, amount of substance (N), pressure (P) and temperature (T) are conserved) followed at 293 K and 1 bar pressure. The temperature coupling at both *NVT* and *NPT* steps used V-rescaling algorithm with a  $\tau_T = 0.1$  ps time constant, using all molecules divided in roughly into two equal groups as the coupled groups. The pressure coupling for the *NPT* run was done using a Berendsen algorithm, with a time constant  $\tau_p = 2$  ps, and isothermal compressibilities taken from a variety of sources. A Verlet cutoff scheme for the both *NVT* and *NPT* runs were used. Particle Mesh Ewald (PME) algorithm was used for electrostatic interactions, with a 1.2 nm cutoff and using 4th order cubic interpolation with 0.16 nm grid spacing for Fast Fourier Transform. A 1.2 nm cutoff was also used for van der Waals interactions. The resulting equilibrated box of solvent molecules was further used for placing the protein.

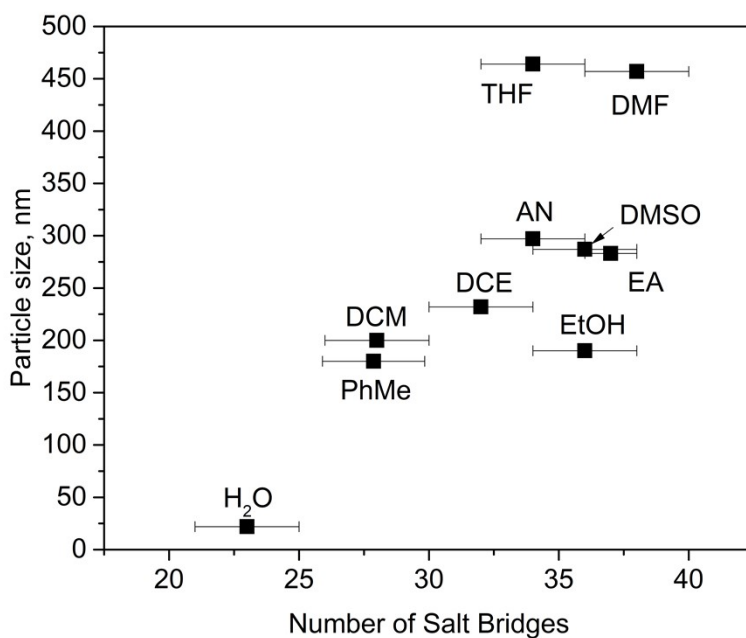


Figure S3. The computed number of salt bridges correlation to the particle size of the aggregated GOx.

The GOx from *Aspergillus niger* structure (PDB entry: 3QVP)<sup>7</sup> was used as a representative GOx model. GOx monomer was used for the MD simulations instead of the dimer because we were largely interested in solvent behaviour near the active site in the proximity of FAD, and in the flavine groups of FAD in the dimer is >2.5 nm, i.e. the behaviour near the active sites of the constituent monomers can rather safely be considered independent from each other. In addition, this saved significant computational resources. To mimic hydration of the protein, it was decided to include water molecules strongly bound to the protein-FAD complex. For that purpose, 10 ns simulation was set up for the protein in an aqueous environment (using general protocol described for protein below), and the protein-FAD complex and 853 water molecules forming hydrogen bonds with the protein or FAD were selected for further simulations in nonaqueous environments. Results of the simulation were analyzed using UCSF Chimera program v. 1.15.<sup>8</sup>

The periodic protein/solvent simulation box was set to dodecahedral with 10 Å distance between the surface of the box and the nearest protein atom. The negative charge of the protein was neutralized with randomly placed Na<sup>+</sup> ions. The simulation in the aqueous solution additionally included 0.15 M NaCl added as freely floating ions. Energy minimization, *NVT* and *NPT* steps MD were essentially the same as for the pure solvent, except the temperature coupling used protein and non-protein atoms as two coupled groups. The production simulations were 200 ns long, and the snapshots were recorded every 1 ns. The salt bridge analysis of the resulting MD snapshots in the 100–200 ns interval was performed using a custom script: the salt bridge was counted in if the minimum distance between oxygens of the negatively charged sidechains (Asp, Glu) and the nitrogens of the positively charged sidechains (Arg, His, Lys) was less than 3.2 Å. Notably, in the beginning of the run GROMACS, the overwhelming majority of designated histidines are uncharged. However, uncharged histidines often formed hydrogen bonds with negatively charged Asp and Glu during the simulation. It was still counted as salt bridges for counting purposes. In the real system, such neutral histidine in a pair with Glu or Asp will likely be protonated, strengthening the binding between the two residues. However, MD is not able to model change of protonation states of the species in the middle of calculation. Still, the simulations seem to reasonably approximate salt bridge formation even with this approximation. The quantum chemical calculations were carried out with the Spartan'18 program package (Spartan'18 for windows version 1.4.0 Wavefunction, Irvine, CA, USA). These structures of the complexes were optimized using a MP2 method of the Møller–Plesset's perturbation theory and a 6-311G(d,p) basis set. To calculate the energy of the hydrogen-bonding interaction between the H-bonded fragments, the standard energy difference method was applied. The basis set superimposition error (BSSE) in calculating the energy difference was corrected by applying the

counterpoise procedure to compute the H-bond energies, in which the virtual orbitals of the other fragment were included in the basis functions.<sup>9</sup> MP2/6-311++G(d,p) as the best method employed in the literature was used for the single points calculations.<sup>10</sup>

## References:

- 1 D. G. Hatzinikolaou and B. J. Macris, *Enzyme Microb. Technol.*, 1995, **17**, 530–534.
- 2 B. Solomon, N. Lotan and E. Katchalski-Katzir, *Biopolymers*, 1977, **16**, 1837–1851.
- 3 M. J. Abraham, T. Murtola, R. Schulz, S. Páll, J. C. Smith, B. Hess and E. Lindahl, *SoftwareX*, 2015, **1–2**, 19–25.
- 4 J. Huang, S. Rauscher, G. Nawrocki, T. Ran, M. Feig, B. L. de Groot, H. Grubmüller and A. D. MacKerell, *Nat. Methods*, 2017, **14**, 71–73.
- 5 K. Vanommeslaeghe, E. Hatcher, C. Acharya, S. Kundu, S. Zhong, J. Shim, E. Darian, O. Guvench, P. Lopes, I. Vorobyov and A. D. Mackerell Jr., *J. Comput. Chem.*, 2010, **31**, 671–690.
- 6 A. Aleksandrov, *J. Comput. Chem.*, 2019, **40**, 2834–2842.
- 7 P.-R. Kommoju, Z. Chen, R. C. Bruckner, F. S. Mathews and M. S. Jorns, *Biochemistry*, 2011, **50**, 5521–5534.
- 8 E. F. Pettersen, T. D. Goddard, C. C. Huang, G. S. Couch, D. M. Greenblatt, E. C. Meng and T. E. Ferrin, *J. Comput. Chem.*, 2004, **25**, 1605–1612.
- 9 S. F. Boys and F. Bernardi, *Mol. Phys.*, 1970, **19**, 553–566.
- 10 D. Tzeli, G. Theodorakopoulos, I. D. Petsalakis, D. Ajami and J. Rebek, *J. Am. Chem. Soc.*, 2011, **133**, 16977–16985.